Construction and Building Materials 362 (2023) 129554

Contents lists available at ScienceDirect

Construction and Building Materials

journal homepage: www.elsevier.com/locate/conbuildmat

Mortar cure-dependent effects on adhesive anchor systems loaded in tension

Stefan Meißl [a], Krešimir Ninčević [a], Bilen Emek Abali [a,b], Roman Wan-Wendner [a,c,*]

[a] Christian Doppler Laboratory LiCRoFasT, University of Natural Resources and Life Sciences Vienna, Peter-Jordanstr. 82, 1190 Vienna, Austria
[b] Division of Applied Mechanics, Department of Materials Science and Engineering, Uppsala University, Box 534, 751 21 Uppsala, Sweden
[c] Magnel Laboratory for concrete research, Department of Structural Engineering, Ghent University, Tech Lane Ghent Science Park - Campus A, Technologiepark-Zwijnaarde 904, 9052 Ghent, Belgium

ARTICLE INFO

Keywords:
Bonded anchors
Adhesive anchors
Mortar cure dependence
Mortar aging influence

ABSTRACT

This paper presents a large experimental campaign and the corresponding analysis quantifying mortar curing effects on the pull-out performance of bonded anchor systems. Standard confined pull-out tests were performed on two commonly used adhesive anchor systems. The two investigated bonded anchor systems were based on different materials, where the mortar of the first bonded anchor system (BAS-VE) was a vinyl-ester based product and the second bonded anchor system (BAS-EP) contained an epoxy-based mortar. In order to isolate the mortar curing effects on the anchor performance, a mature concrete was used as base material minimizing well-known aging and curing effects related to the substrate, concrete. In total, 93 pull-out tests were performed for various curing times in order to characterize influences on bond strength, stiffness, and peak displacement. Depending on the product specifications and corresponding approval documents, tests were carried out in a time-range of a few minutes up to three months after the anchor installations. Measured temperature (and humidity histories) of the environment have been utilized for predicting the mortars' degree of cure for each structural anchor test. The results show a cure-dependent behavior in BAS-VE and BAS-EP. Although the bond strength fails to increase significantly after reaching the manufacturer approved minimum curing time, the stiffness shows an increase for longer cured anchors.

1. Introduction

Post-installed anchor systems are widely used in the construction industry. Beside traditional, cast-in-place anchors, like headed studs, post-installed anchors are a modern method, yet one of indispensable fastening methods in the structural engineering field. Advantages of post-installed fasteners lie in the possibility of applying them for retrofitting and rehabilitation purposes as well as using them as a flexible and sustainable design and construction [1,2]. In general, mechanical post-installed anchors, like undercut- and expansion systems, encompass a steel fastener inserted in a pre-drilled borehole in base-material (concrete or brick-stone). In bonded anchor systems, a third component is involved, namely an adhesive mortar. This setting is mainly used for facades, tunnel and bridge constructions. In this three-component bonded anchor system, the working principle relies on bond, where the adhesive mortar layer transfers the load from the steel rod to the concrete along the entire bonded length [2]. While the apparent adhesion due to mechanical interlocking [3] provides limited shear stress transfer only, gluing the steel rod to the concrete leads to improved bond [4–6]. The installation of bonded anchor systems comprises straight-forward steps—these steps are also included in user manuals from manufacturer of adhesive mortars. After drilling and cleaning the borehole, the adhesive mortar is filled in and the threaded bar is inserted. Material response varies in time, mostly because of time-dependent effects like curing and aging. For the concrete response, ample studies indicate a change in material response, mainly depending on the hygro-thermal boundary conditions of the structure [7–14]. This change is an increase in stiffness, quite substantial at an early age and levels off at more mature ages. Numerical approaches exist that capture aging related phenomena of concrete [12,15–19]. Reaching accurate predictions of the design-life, a number of phenomena need to be considered in concrete, caused by concrete-hydration [20], internal friction during deformation [21,22], mechanical response change due to the loading rate [23,24] or concrete damage [8,18,25]. In the fastening specific case, without involvement of adhesives, the age and cure-dependency has been experimentally investigated in [26–30] for undercut and headed studs. In the case of the adhesive mortar, time-dependent changes in mechanical properties have been analyzed

* Corresponding author at: Magnel Laboratory for concrete research, Department of Structural Engineering, Ghent University, Tech Lane Ghent Science Park - Campus A, Technologiepark-Zwijnaarde 904, 9052 Ghent, Belgium.
E-mail address: roman.wanwendner@ugent.be (R. Wan-Wendner).

https://doi.org/10.1016/j.conbuildmat.2022.129554
Received 24 April 2022; Received in revised form 20 October 2022; Accepted 21 October 2022

in [31,32] with the conclusion that both investigated adhesive materials (vinyl-ester-based and epoxy-based mortars) show significant changes due to post-curing, hydrolytic effects, and phase change. More experimental results on the mechanical response of polymer composite materials are reported in [33–35] for short- and long term [36], respectively. The age of the concrete is only loosely regulated by current design codes and approvals, as base-material for bonded anchors. However, the minimum curing time of the mortar is recommended by the manufacturer. The suggested curing times depend on the adhesive material as well as manufacturer. In general, concrete as base-material for fastening applications, must be older than 21 days and may not exceed an age of 18 month to determine the bond properties of adhesive anchor systems [29]. Beside the curing process, it is well known that the involved materials – and in turn, the anchors' system performance – are affected by long-term phenomena [34,36,37] like creep and shrinkage [29,38,39] Owing to the chemical hardening via crosslinking, vinyl-ester based mortars reach their minimum curing time faster, at around 1 to 2 h, while for epoxy based mortars it takes around 10 to 12 h at room temperature. Also the type of application plays a role for the minimum curing time. A sizable range of applications exists, from the typical installation of a threaded bar in concrete to systems approved in brick-stones, for reinforcement connections, at specific boundary conditions, like high and low temperatures, or for applications in a humid environment or even under water use.

Overall, temperature highly affects the curing time of bonded anchor systems, since the curing rate depends on temperature. In this study, we investigate two bonded anchor systems, BAS-VE and BAS-EP, and analyze how the two bonded anchor systems perform in standard confined pull-out tests at different times after installation. In order to isolate the effects on the response coming from aging of the mortar, it is necessary to minimize concrete aging effects by using a mature concrete as base-material. In addition, for both adhesive mortars a numerical model was developed in order to compute the degree of cure of the adhesive for each individual pull-out test.

2. State of the art

The determination of the ultimate load capacity of bonded fasteners in concrete is regulated by EAD 330499-01-0601 - BONDED FASTENERS FOR USE IN CONCRETE [40]. The corresponding technical report (TR048 - Details of tests for post-installed fasteners in concrete) [41] prescribes details for the two distinguished testing methods. In both cases, a threaded rod, installed in an un-reinforced, un-cracked concrete slab is loaded in tension until failure. The so called "unconfined test setup" reproduces the anchor case at construction sites realistically, since the supports allow an unrestricted formation of a concrete cone. The confined test setup on the other side aims at avoiding concrete cone failure and is governed by failure in or close to the mortar layer. In order to generate this so-called pull-out" failure, the supports are moved close to the anchor rod, leading to a "confinement". In general a circular, confinement plate made from steel is positioned below the supports of the testing-machine in order to ensure a uniform confinement stress distribution around the anchor rod. According to TR048 [41], the confinement plate has to be stiff, and the area of support should avoid a large compression of the concrete. The recommendation is to keep the occurring compressive stresses below 70% of the concrete compressive strength. This condition is achieved by the design of the outer diameter of the plate. The diameter of the centered through-hole should have a borehole-diameter d_0 + 4 mm. Besides pull-out failure, there are other failure modes [1]:

- steel failure in the anchor,
- concrete splitting failure,
- concrete breakout,
- and the combined pull-out and concrete failure.

The mixed mode failure is a combination of concrete breakout at the upper part along the anchor rod and pull-out failure at the bottom of the anchor. This failure mode usually occurs in the unconfined test setup [42].

For a better phenomenological understanding, it is possible to select the concrete members as base-material, the anchor position, the anchor rods dimensions, and material and tune the test setup in such a way that a specific failure mode is triggered. In the real fastening situation, reinforcement steel minimizes splitting of the base material. However, confined pull-out tests are performed in un-reinforced concrete, where manufacturer-recommended geometries and distances are adhered.

Over the last years a number of empirical models have been developed in order to estimate the pull-out capacity of fasteners, which can be used for design [42,43]. The uniform bond model as in [2] provides the best fit based on a large database of bonded anchors and is recommended by current international standards to estimate the pull-out capacity. In this model, the shear stress along the anchor is assumed to be constant. Eq. (1) shows how the expected pull-out load N_u [kN] is calculated, based on the bonded length h_{ef} [mm], the borehole diameter d_0 [mm], and the bond resistance, which is defined as the bond strength τ_0 [MPa] of the adhesive anchor system, as follows:

$$N_u = \tau_o d_0 \pi h_{ef} \tag{1}$$

As an alternative, the anchor diameter, d, together with the related bond strength, τ, may be used in the equation, which shows an even better prediction [43]. An experimental validation in [44] indicates that $d_0 < 1.5d$ and $4.5 < h_{ef}/d < 20$ are necessary conditions to be fulfilled.

3. Materials used in experiments

In total the experimental campaign comprises 93 confined pull-out tests. The anchor tests were carried out by varying the curing times, which are compiled in Tables 6 and 7. The concrete properties alter over the age. We use such a model in order to check the significance of concrete dependent response change. Two adhesive mortars are involved in the investigations herein. In BAS-VE a vinyl-ester based mortar is used, BAS-EP includes an epoxy-based mortar. Their characteristics are fundamentally different.

3.1. Anchor type

Both investigated bonded anchor systems comprised M16 threaded bars made from 10.9 steel class as fastening elements. The design of the threaded rods was based on the uniform bond model (1), such that steel failure is avoided. Furthermore, this model allows to estimate the pull-out capacity of the corresponding anchor geometry and configuration. The required bond strength values, τ, were informed by experiences made in previously performed experimental tests on the vinyl-ester and epoxy based anchor systems and lead to a bonded length h_{ef} of 80 mm for BAS-VE and 64 mm for BAS-EP, respectively. Fig. 1 shows a schematic sketch of the bonded anchor systems with the corresponding bonded lengths . Both bonded lengths represent the minimum approved lengths h_{ef}.

3.2. Vinyl-ester mortar (BAS-VE)

The vinyl-ester mortar comprises a dibenzoyl peroxide hardener. The inorganic filler material – mainly quartz and cement – is of a relatively high amount around 20 to 50 vol-% [31]. The curing kinetics are quick. Table 1 gives an overview of the manufacturer approved minimum curing times at the corresponding temperatures of the base-material.

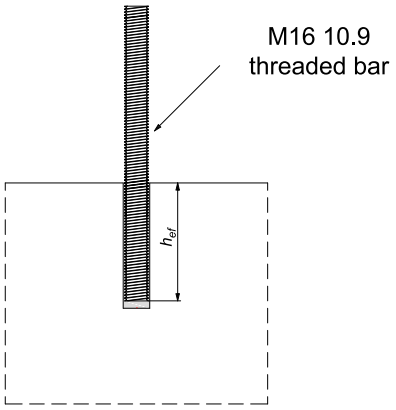

Fig. 1. Bonded length h_{ef} for BAS-VE: 80 mm and BAS-EP: 64 mm.

Table 1
Manufacturer approved curing times for BAS-VE.

Temperature range	Curing time t_{cur}
−5 - ±0 °C	24 h
+1–+5 °C	3 h
+6–+10 °C	90 min
+11–+20 °C	60 min
+21–+30 °C	45 min
+31–+40 °C	35 min

Table 2
ETA approved curing times for BAS-EP.

Temperature range	Curing time $t_{cur.ini}$	Curing time $t_{cur.full}$
5 °C–9 °C	≥18 h	≥72 h
10 °C–14 °C	≥12 h	≥48 h
15 °C–19 °C	≥8 h	≥24 h
20 °C–29 °C	≥6 h	≥12 h
30 °C–39 °C	≥4 h	≥8 h
40 °C	≥2 h	≥4 h

Table 3
Manufacturer approved curing times for BAS-EP.

Temperature range	Curing time $t_{cur.ini}$	Curing time $t_{cur.full}$
−5 °C - −1 °C	≥36 h	≥72 h
0 °C–9 °C	≥25 h	≥50 h
10 °C–19 °C	≥12 h	≥24 h
20 °C–29 °C	≥6 h	≥12 h
30 °C–39 °C	≥4 h	≥8 h
40 °C	≥2 h	≥4 h

3.3. Epoxy mortar (BAS-EP)

The used, commercially available, epoxy mortar is a compound of a polymer matrix with a relatively high amount inorganic, broken fillers. For enhancing product properties different filler materials are mixed in the mortar. The mortar is based on a bisphenol A/F epoxy resin with an amine hardener. [31]

Tables 2 and 3 show the curing times specified by the manufacturer's manual for BAS-EP. The minimum curing times in Table 2 are declared as approved by ETA, while the minimum curing times reported in Table 3 are slightly different and adequate only in a dry base-material. Different to BAS-VE, the manufacturer of BAS-EP specifies a minimum "initial" curing time, $t_{cure,ini}$, and a minimum "full" curing time, $t_{cure,full}$, in the corresponding installation manual.

3.4. Concrete

All pull-out tests were performed on two concrete slabs cast from one batch. These concrete members had a length L=2500 mm, a width W=1000 mm, and a thickness H=300 mm. After casting, the slabs were stored outside the laboratory, close to each other. 24 h before the anchor installation, they were moved inside the laboratory. Environmental conditions, like temperature and humidity, were fully recorded from the time of casting until the end of the campaign. Table 4 shows the detailed concrete mix design.

Table 4
Concrete mix design.

Mix design parameters	Units	Concrete
Cement	[kg/m^3]	275.20
Cement type	[–]	CEM II 42.5 N
Coarse aggregate type	[–]	limestone
Aggregate shape	[–]	round
Max. aggregate Size	[mm]	16
Fine aggregates 0–4 mm	[kg/m^3]	1236.90
Total amount aggregates	[kg/m^3]	2067.00
Water	[kg/m^3]	173.70
Superplasticizer	[kg/m^3]	1.65
Retarder	[kg/m^3]	1.37
Water cement ratio w/c	–	0.63
Aggregate cement ratio a/c	–	7.51

As reported in [12,28] concrete curing leads to quite significant changes in the concrete properties and pull-out capacity on mechanical anchors. It is obvious that concrete related curing effects may mask the cure-dependent changes in the adhesive mortar. This situation leads then to smeared out effects on the system response and makes an analysis very challenging. Luckily we know from observations in [7] that cure-dependent property changes occur especially at young concrete ages and die out for older concretes.

In order to remove effects related to concrete aging, a mature concrete member is used, hopefully minimizing the concrete specific aging effects. Specifically, the installation of the bonded anchors was done in an age range from 351 to 391 days after concrete casting. Furthermore, in order to ensure that the chosen age was adequate, a full concrete characterization was performed at different concrete ages. 28 days after casting the compression tests were performed on concrete cubes, while the full characterization by means of cube compressive strength, f_{cu}, cylinder compressive strength, f_{cy}, Brazilian splitting indirect tensile strength, $f_{t,B}$, and elastic modulus, E, were carried out at a concrete age of 36 days. In addition, the full characterization was repeated 85 and 273 days after casting. Cubical and cylindrical specimen for concrete characterization were stored next to the slabs as requested in [40] to ensure equal curing conditions. Aging functions reported in Eurocode [45] and modelcode [46] were used for estimating the aforementioned concrete properties at the specific age when the pull-out tests were performed (Eq. (2)).

$$f_c = f_{c,28}\exp\left(s(1-\sqrt{28/t})\right), \tag{2}$$

The parameter s, which according to Eurocode 2 depends on the cement type, was fitted on the experimental characterization values and used for the estimation of the corresponding properties at 351 and 478 days of concrete age. Table 5 summarizes the experimentally obtained and the estimated (*) properties for the considered concrete ages. In order to validate the proposed aging function, the concrete properties were calculated for a concrete age of 84 and 274 days based on the 28 and 36-day values. As seen in Table 5, experimentally determined and calculated values for 84 and 274 days show good agreement. Comparing the properties between each other, for the ages where pull-out tests were carried out, we conclude that aging effects indeed were insignificant within the time-range of the test campaign.

4. Experiments

For BAS-VE 54 tests and BAS-EP 39 tests were carried out in total. In order to avoid influences from local properties in the concrete slab,

Table 5
Summary of concrete properties from different specimens and ages. Prediction according to Eurocode aging functions. (*...predicted)

Concrete age Days	f_{cu} MPa	f_{cy} MPa	E GPa	$f_{t,B}$ MPa
s	0.22	0.15	0.16	0.27
28	36.99 ± 1.20%	-	-	-
36	-	39.34 ± 2.10%	32.09 ± 4.30%	4.20 ± 5.20%
84	40.77 ± 1.80%	41.35 ± 4.20%	33.06 ± 4.20%	4.70 ± 3.30%
84	40.66*	41.25*	33.49*	4.61*
232	42.68 ± 1.18%	-	-	-
274	-	42.76 ± 3.70%	35.05 ± 9.00%	4.90 ± 3.60%
274	43.03*	42.88*	34.91*	4.94*
351	43.39*	43.12*	35.11*	4.99*
478	43.77*	43.38*	35.34*	5.04*

*Predicted.

Table 6
Overview of pull-out tests for BAS-VE at different curing times.

Label	Repetitions	Label	Repetitions
BAS-VE_8min	1	BAS-VE_10h	1
BAS-VE_12min	1	BAS-VE_12h	1
BAS-VE_15min	1	BAS-VE_14h	1
BAS-VE_22min	1	BAS-VE_15h	1
BAS-VE_30min	1	BAS-VE_16h	1
BAS-VE_45min	2	BAS-VE_20h	2
BAS-VE_60min	1	BAS-VE_22h	1
BAS-VE_90min	1	BAS-VE_1d	5
BAS-VE_100min	1	BAS-VE_4d	5
BAS-VE_120min	1	BAS-VE_1w	5
BAS-VE_180min	1	BAS-VE_3w	1
BAS-VE_200min	1	BAS-VE_1m	5
BAS-VE_4h	1	BAS-VE_3m	5
BAS-VE_4.5h	1		
BAS-VE_5h	2		
BAS-VE_6h	1		
BAS-VE_7h	1		
BAS-VE_8h	1		

Table 7
Overview of pull-out tests for BAS-EP at different curing times.

Label	Repetitions	Label	Repetitions
BAS-EP_3.5h	1	BAS-EP_14h	1
BAS-EP_4h	1	BAS-EP_15h	2
BAS-EP_4.5h	1	BAS-EP_16h	1
BAS-EP_5h	1	BAS-EP_18h	1
BAS-EP_5.5	1	BAS-EP_20h	1
BAS-EP_6h	1	BAS-EP_22h	1
BAS-EP_6.5h	1	BAS-EP_1d	5
BAS-EP_7h	1	BAS-EP_1w	5
BAS-EP_8h	1	BAS-EP_1m	5
BAS-EP_10h	1	BAS-EP_3m	5
BAS-EP_12h	1		
BAS-EP_13h	1		

the different tests were randomly distributed on two concrete slabs of the same batch, while minimum edge distances (BAS-VE: 65 mm, BAS-EP: 50 mm) and minimum spacing values (BAS-VE: 65 mm, BAS-EP: 75 mm) were adhered to prevent edge effects and impacts from neighboring tests.

4.1. Anchor installation

24 h before installation, the concrete slabs were put inside the laboratory. To ensure a sufficient temperature of the base material, approved by manufacturers, the core temperature of the slabs was measured by a thermocouple type K. Before installation of the first anchors, the core temperature was already beyond 20°C. The anchor installation was systematically performed by following the manufacturer specific approval guidelines. After drilling the borehole by using a rotary hammer drill-bit, the borehole was cleaned according to manufacturer guidelines. With the help of a drill stand, the borehole-axis was ensured to be perpendicular to the concrete surface. After the boreholes were cleaned for installation, the mortar was injected into the borehole, from the bottom to the top to avoid bubbles in the mortar. Bubbles may alter the pull-out capacity by an unknown extent. Subsequently, the threaded bar was pressed inside the borehole accompanied by a rotation, this helical motion distributes the mortar along the bar adequately.

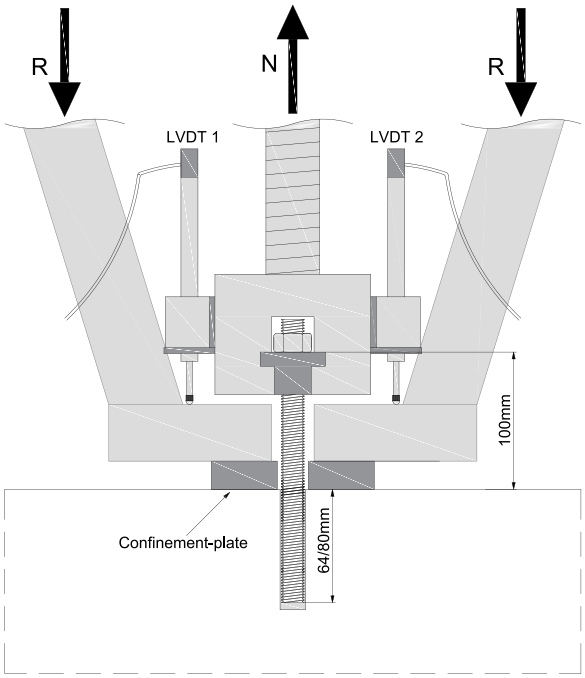

Fig. 2. Confined test setup.

4.2. Testing procedure

All tests were performed following the EAD guidelines [40] An overview of the confined pull-out setup is shown in Fig. 2.

The round confinement-plate prevents the concrete slab from lifting during the test. This 25 mm thick steel plate has an outer diameter of 115 mm, and a center-hole-diameter of 22 mm. In all tests, the load, N, was applied consistently at the top of the bonded anchor, at a distance of 100 mm from the concrete surface, to ensure full comparability of the results. To minimize bending-moment influences, a spherical coupling was used between machine-actuator and anchor connection. The tests were performed under quasi-static loading by a 630 kN servo-hydraulic jack, while a linear variable differential transducer (LVDT) was used to ensure the test-stability by prescribing a constant displacement rate of 0.01 mm/s, to reach the peak within 1 to 3 min. A close position of

the differential transducer to the concrete surface reduced the danger of snap-back during the test. In addition, a second LVDT was mounted to the steel-grip, to measure the displacement on the second side. For an increased accuracy in measuring the actual anchor response, LVDT 1 and LVDT 2 were simultaneously recorded and their mean value was later used in analysis.

4.3. Default curing times

Two bonded anchor systems, BAS-VE and BAS-EP, comprising different mortar materials were investigated. Referring to the fully recorded temperature history during the campaign, reaching from 21 °C to 30°C, the minimum approved curing times are defined at 45 min for BAS-VE and 12 h for BAS-EP. Curing times at specific temperature values are reported in Table 6 for BAS-VE and in Table 7 for BAS-EP. Beside the approved tests, which were performed respecting the given manufacturer times, ample tests were intentionally performed neglecting the minimum curing time, in order to establish a cure-dependent dataset. These testing times reached from the earliest possible to the minimum approved curing time and beyond to a maximum age of 3 month. For BAS-VE the first test was carried out 8 min after installation. For BAS-EP the first test could be performed 3.5 h after installation. This difference is the result of differences in the curing kinetics of vinyl-ester based thermoset BAS-VE and epoxy based thermoset BAS-EP. Due to logistical limitations, for both anchor systems single tests were performed at predefined curing times, reaching from the shortest curing time possible up to 22-hour tests.

For BAS-VE, 28 single tests were performed up to a curing time of 22 h. The curing differences for the young ages (<5 h) were in a 4-to-60-minute range and the tests performed after 5 h had 60-to-120-minute steps. To investigate the scatter and determine unknown long-term trends, at 1 day, 4 days, 1 week (7 days), 1 month and 3 months; 5 repeating pull-out tests were performed. Table 6 gives a detailed overview of all performed pull-out tests at the given curing times for BAS-VE.

BAS-EP comprised 19 single tests up to a curing time of 22 h, where the time-steps were increasing by half an hour for the young ages (3.5 to 7 h) and in steps of one or two hours for the more mature curing times (7 to 22 h). Additionally, at 1 day, 1 week (9 days), 1 month and 3 months; 5 test repetitions were carried out. Table 7 summarizes the detailed curing times for BAS-EP.

4.4. Temperature and humidity recordings

Over the whole time of the experimental campaign, ambient temperature and humidity were recorded next to the concrete slabs. Furthermore, thermocouples were installed into pre-drilled boreholes and then sealed in order to record the core temperature in a depth of around 50 mm. Hence, temperature of the concrete member was measured during the anchor installation and the pull-out procedure. Fig. 3 summarizes the temperature history including both the core temperature (plotted in black) and ambient temperature (green). It is noted that although both temperature-histories are close, the ambient temperature exceeded the core temperature by as much as +8.5°C. This value was measured before anchor installation on 2020-05-26 16:14. The contrary maximum deviation, when ambient temperature was 5.89 degree below core temperature, was detected on 2020-07-03 08:22. The blue circles mark the installation points and the red dots label the instant of the anchor tests. In spite of the big temperature drop on September 2020, which occurred before the last tests, no influences on the pull-out tests are expected, since the base-material concrete had already reached a very mature age at this point in time (474 days). Detailed information by means of the temperature and humidity at installation and testing is provided in the Annex (Tables 10, 11, 12 and Fig. 7).

4.5. Mortar curing and modeling degree of cure

In both investigated bonded anchor systems, thermosetting polymers are applied. To unify the experimental results independent of the temperature, modeling the degree of cure of these thermosetting polymers allowed to map time at a variable temperature into a curing degree evolution. Vinyl-ester based and epoxy based, so-called two component thermosetting polymers are adiabatic catalytic systems. With mixing the two components curing starts as an exothermal reaction. The produced heat is then used to continue the curing process. This reaction stops once curing is completed. Curing is a hardening process linked to crosslinking between polymer chains. The process of curing can be observed either experimentally [47], or numerically. We refer to [48] for a general framework of modeling and computational implementation in thermo-mechano-chemical processes.

Different modeling approaches exist, for example in mechanical characterization [49], thermomechanical consideration [50], especially below the gel point [51,52], or considering aging [53,54] along the curing process. Beside simple linear models, various models have been investigated by exploiting numerical multi-scale approaches [55–57]. In addition, multiphysics approaches with numerical implementations [58] are developed for thermo-setting materials assuming small [59,60] or large displacements [61–63], which have been applied in several applications [64–66], where the curing process took place in controlled environmental conditions.

Especially with crosslinking beyond a so-called gelation point, the more structured polymer chains act stiffer. This hardening process causes shrinkage leading to residual stresses [67] and can be measured while the liquid resin increases its viscous response until the gelation point. Beyond that a solid is formed and moduli are measured. This process is often characterized by a degree of cure, ϕ, between 0 and 1. Modeling of this process is based on theory of mixtures, where hardened and yet to be hardened phases constitute the material. The degree of cure, ϕ, denotes the ratio of hardened material in the bulk. Its change in time is modeled by an evolution equation and a coupled thermomechanical simulation is possible with material equations derived by using principles of thermodynamics [48,60,68]. Modeling the evolution equation for the degree of cure is based on the type of chemical reaction kinetics. Based on the vinyl-ester material, BAS-VE consists of autocatalysis and impurity catalysis. Reaction kinetics [69] based on an autocatalysis mechanism leading to a so-called Kamal's equation [70], as follows:

$$\begin{aligned} \dot{\phi} &= (k_1 + k_2\phi^m)(1-\phi)^n \,, \\ k_1 = A_1 \exp\!\left(-\frac{E_1}{RT}\right), k_2 &= A_2 \exp\!\left(-\frac{E_2}{RT}\right) . \end{aligned} \tag{3}$$

Kinetic rate coefficients, k_1 and k_2, are modeled by A_1, E_1 and A_2, E_2, respectively. As usual, an Arrhenius relation is utilized with the gas constant $R = 8.314\,\mathrm{J/(mol\,K)}$. Catalysis is a chemical process modeled by power laws, m and n are parameters to be determined. We refer to [71, Table 1] for a collection of such parameters.

For BAS-EP, Kamal's equation is insufficient for modeling [72,73]. Here, a so-called glass transition temperature, T_g, affects the material response. In the case of decreasing temperature, the material goes from a rubbery state to a glassy state. Below and above glass transition temperature, different mechanisms dominate the curing process. Mainly the model is based on the assumption that diffusive and chemically steered mechanisms act together [74], which are introduced by [75] based on phenomenological observations combined with the free volume reduction during curing. In the glassy state, the diffusion rate approaches zero with respect to the chemical rate. As is the nature of an autocatalytic reaction, the process never stops, but practically the rate is zero, which is called a partial freeze or vitrification. The glass transition temperature is modeled accurately by a fit function, depending only on the temperature [76], based on calorimetric measurements. We follow [77,78] and use

$$T_g = \exp\!\left(\frac{(1-\phi)\ln(T_{g,0}) + \Delta C\phi \ln(T_{g,\infty})}{(1-\phi) + \Delta C\phi}\right) , \tag{4}$$

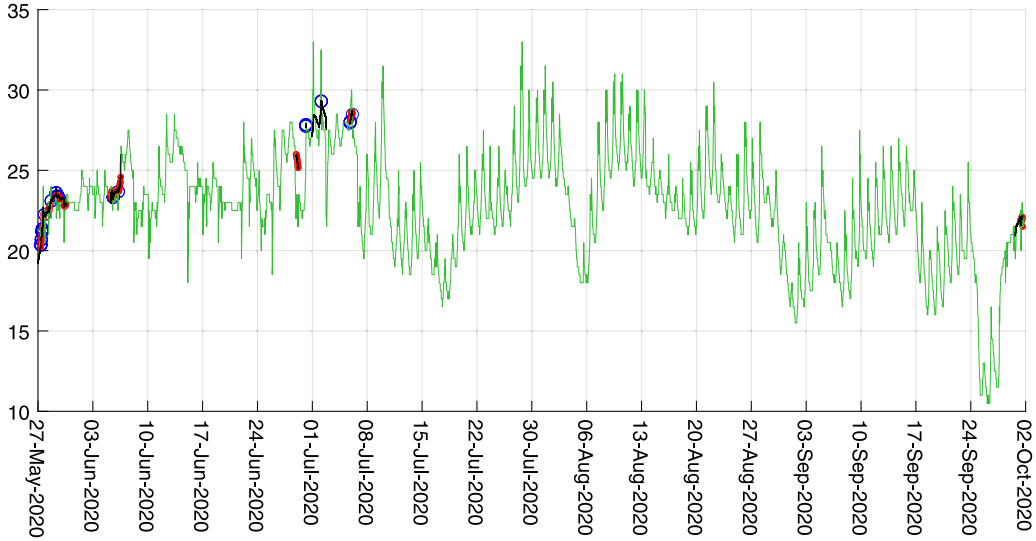

Fig. 3. Recorded core (black)- and ambient (green, largely overlapping the core temperature) temperature history during full campaign. The blue circles mark the installation points and the red dots label the instant of the anchor tests. Enlarged figures are provided in the Annex 8(a), 8(b), 8(c). (For interpretation of the references to color in this figure legend, the reader is referred to the web version of this article.)

Table 8
Experimental response by means of pull-out force, bond strength, secant stiffness (determined between 30 and 60% of ultimate load) and displacement@peak for BAS-VE.

Label	Repetitions	Pull-out force $N_{exp.}$ kN	Bond strength $\tau_{exp.}$ MPa	Stiffness K kN/mm	Displacement @peak mm
BAS-VE_8min	1	66.28	16.48	71.51	1.38
BAS-VE_12min	1	71.50	17.78	65.00	1.45
BAS-VE_15min	1	83.23	20.70	73.09	1.71
BAS-VE_22min	1	81.52	20.27	74.34	1.42
BAS-VE_30min	1	85.92	21.37	83.93	1.81
BAS-VE_45min	2	76.38 ± 16.96%	18.99 ± 16.96%	82.63 ± 10.69%	1.24 ± 1.40%
BAS-VE_60min	1	91.34	22.71	88.98	1.39
BAS-VE_90min	1	89.40	22.23	84.30	1.29
BAS-VE_100min	1	76.77	19.09	79.50	1.23
BAS-VE_2h	1	83.82	20.84	86.00	1.23
BAS-VE_3h	1	87.25	21.7	82.21	1.34
BAS-VE_200min	1	87.47	21.75	89.25	1.20
BAS-VE_4h	1	89.17	22.17	88.21	1.22
BAS-VE_4-5h	1	82.17	20.43	89.49	1.18
BAS-VE_5h	2	83.57 ± 9.23%	20.78 ± 9.23%	96.47 ± 4.90%	1.06 ± 5.08%
BAS-VE_6h	1	77.02	19.15	96.47	0.98
BAS-VE_7h	1	86.53	21.52	88.13	1.16
BAS-VE_8h	1	94.77	23.57	98.20	1.16
BAS-VE_10h	1	91.56	22.77	81.14	1.30
BAS-VE_12h	1	95.19	23.67	102.18	1.33
BAS-VE_14h	1	82.89	20.61	79.01	1.51
BAS-VE_15h	1	99.94	24.85	97.59	1.24
BAS-VE_16h	1	102.88	25.58	93.22	1.17
BAS-VE_20h	2	102.80 ± 3.57%	25.56 ± 3.57%	98.23 ± 17.36%	1.20 ± 16.45%
BAS-VE_22h	1	96.84	24.08	100.23	1.16
BAS-VE_1d	5	89.28 ± 12%	22.20 ± 12%	93.50 ± 8.60%	1.12 ± 6.75%
BAS-VE_4d	5	86.36 ± 11.35%	21.48 ± 11.35%	99.42 ± 4.09%	1.07 ± 9.76%
BAS-VE_1w	5	90.66 ± 6.70%	22.54 ± 6.70%	92.31 ± 10.84%	1.22 ± 15.62%
BAS-VE_3w	1	103.71	25.79	129.28	0.94
BAS-VE_1m	5	93.49 ± 8.7%	23.25 ± 8.70%	119.71 ± 12.76%	0.97 ± 17.16%
BAS-VE_3m	5	87.85 ± 11.17%	21.85 ± 11.17%	126.33 ± 16.85%	0.99 ± 20.07%

with $\Delta C = \Delta c_\infty / \Delta c_0$ as the ratio of the heat capacity change at the glass transition. Mobility plays a dominant role in the rubbery state and the kinetic rate is so high, we practically observe hardening solely above T_g. As introduced in [77], we use only primary and secondary amines via autocatalysis and impurity catalysis (denoted by c in index), collective kinetic rates, K_1, K_{1c}, which involve a diffusion controlled mechanism, K_{diff}, as well as a chemically steered mechanism, $K_{1,\text{chem}}$, $K_{1c,\text{chem}}$, as suggested in [79]. Finally, we acquire the following evolution equation:

$$
\begin{aligned}
\dot{\phi} &= K_1(1-\phi)^2\left(\phi + \frac{K_{1c}}{K_1}\right), \\
\frac{1}{K_1} &= \frac{1}{K_{1,\text{chem}}} + \frac{1}{K_{\text{diff}}}, \frac{1}{K_{1c}} = \frac{1}{K_{1c,\text{chem}}} + \frac{1}{K_{\text{diff}}}, \\
K_{1,\text{chem}} &= A_3 \exp\left(-\frac{E_3}{RT}\right), K_{1c,\text{chem}} = A_4 \exp\left(-\frac{E_4}{RT}\right), \\
K_{\text{diff}} &= k_{T_g} \exp\left(\frac{C_1(T-T_g)}{C_2 + |T-T_g|}\right).
\end{aligned}
\tag{5}
$$

Table 9
Experimental response by means of pull-out force, bond strength, secant stiffness (determined between 30 and 60% of ultimate load) and displacement@peak for BAS-EP.

Label	Repetitions	Pull-out force $N_{exp.}$ kN	Bond strength $\tau_{exp.}$ MPa	Stiffness K kN/mm	Displacement @peak mm
BAS-EP_3-5h	1	24.96	7.76	1.00	28.59
BAS-EP_4h	1	53.65	16.68	23.25	4.08
BAS-EP_4-5h	1	73.32	22.79	100.48	1.80
BAS-EP_5h	1	84.56	26.29	91.58	1.90
BAS-EP_5-5h	1	90.84	28.24	105.56	0.96
BAS-EP_6h	1	102.20	31.77	104.12	1.10
BAS-EP_6-5h	1	105.82	32.90	103.89	1.02
BAS-EP_7h	1	114.30	35.53	108.96	1.11
BAS-EP_8h	1	111.84	34.76	102.88	1.20
BAS-EP_10h	1	121.16	37.66	115.30	1.10
BAS-EP_12h	1	119.41	37.12	101.33	1.25
BAS-EP_13h	1	109.00	33.88	84.38	1.47
BAS-EP_14h	1	126.32	39.27	106.06	1.26
BAS-EP_15h	2	126.06 ± 0.76%	39.19 ± 0.76%	107.91 ± 0.18%	1.21 ± 6.33%
BAS-EP_16h	1	126.83	39.43	112.27	1.20
BAS-EP_18h	1	128.52	39.95	112.76	1.18
BAS-EP_20h	1	126.12	39.20	121.09	1.11
BAS-EP_22h	1	126.44	39.30	116.83	1.16
BAS-EP_1d	5	123.21 ± 2.57%	38.30 ± 2.57%	101.57 ± 6.93%	1.26 ± 7.17%
BAS-EP_1w	5	128.86 ± 5.65%	40.06 ± 5.65%	102.67 ± 9.28%	1.36 ± 10.86%
BAS-EP_1m	5	124.15 ± 2.47%	38.59 ± 2.47%	139.04 ± 10.14%	1.03 ± 14.85%
BAS-EP_3m	5	126.11 ± 2.14%	39.20 ± 2.14%	137.97 ± 11.12%	1.06 ± 9.22%

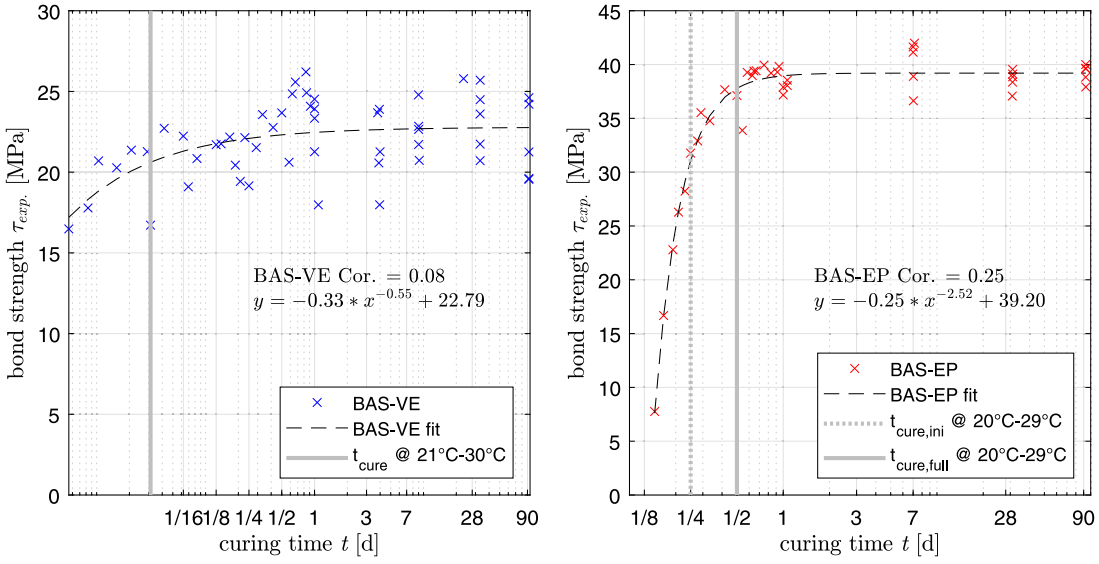

(a) BAS-VE (b) BAS-EP

Fig. 4. Evolution of the cure-dependent capacity by means of bond strength for BAS-VE and BAS-EP. (Vertical gray lines represent the manufacturers' suggested minimum curing times. For BAS-EP the manufacturer defines a "initial" and a "full" curing time). (For interpretation of the references to color in this figure legend, the reader is referred to the web version of this article.)

The diffusion rate, K_{diff}, is modeled by the Williams–Landel–Ferry (WLF) equation in the rubbery regime. This rate is greater than the chemical rate, K_{chem}, in several orders in magnitude. By using standard techniques and a Digital Scanning Calorimeter (DSC), all parameters are determined.

5. Results and discussion

By using the complete experimental data from the structural pull-out tests, we investigate the influence of curing time, thus, degree of cure, on the system response characterized by pull-out capacity, bond strength, secant stiffness (determined between 30 and 60% of ultimate load), and displacement at peak. In Tables 8 and 9, the experimental results for the tests on BAS-VE and BAS-EP respectively, are provided. It is noted, that the large deformation for BAS-EP_3-5h of 28.59 mm comes from the low modulus at a very early mortar age.

5.1. Corrections: Elastic deformation

Since the focus of the current investigation was the influence of the bond behavior, the elastic deformations of the involved parts outside the concrete were removed from the anchor response. Specifically, the elastic strain of the outer part of the threaded bar δ_{TB} and the setup parts (confinement plate and setup-support-plate) δ_{CSP} were calculated to retrieve the elongation according Eq. (6) and (7), respectively and subtracted from the experimental displacement δ_{exp} in (8).

$$\delta_{TB} = \frac{\left(\frac{N_{\text{exp}}}{A_{TB}}\right)}{E_{TB}} l_{TB} \tag{6}$$

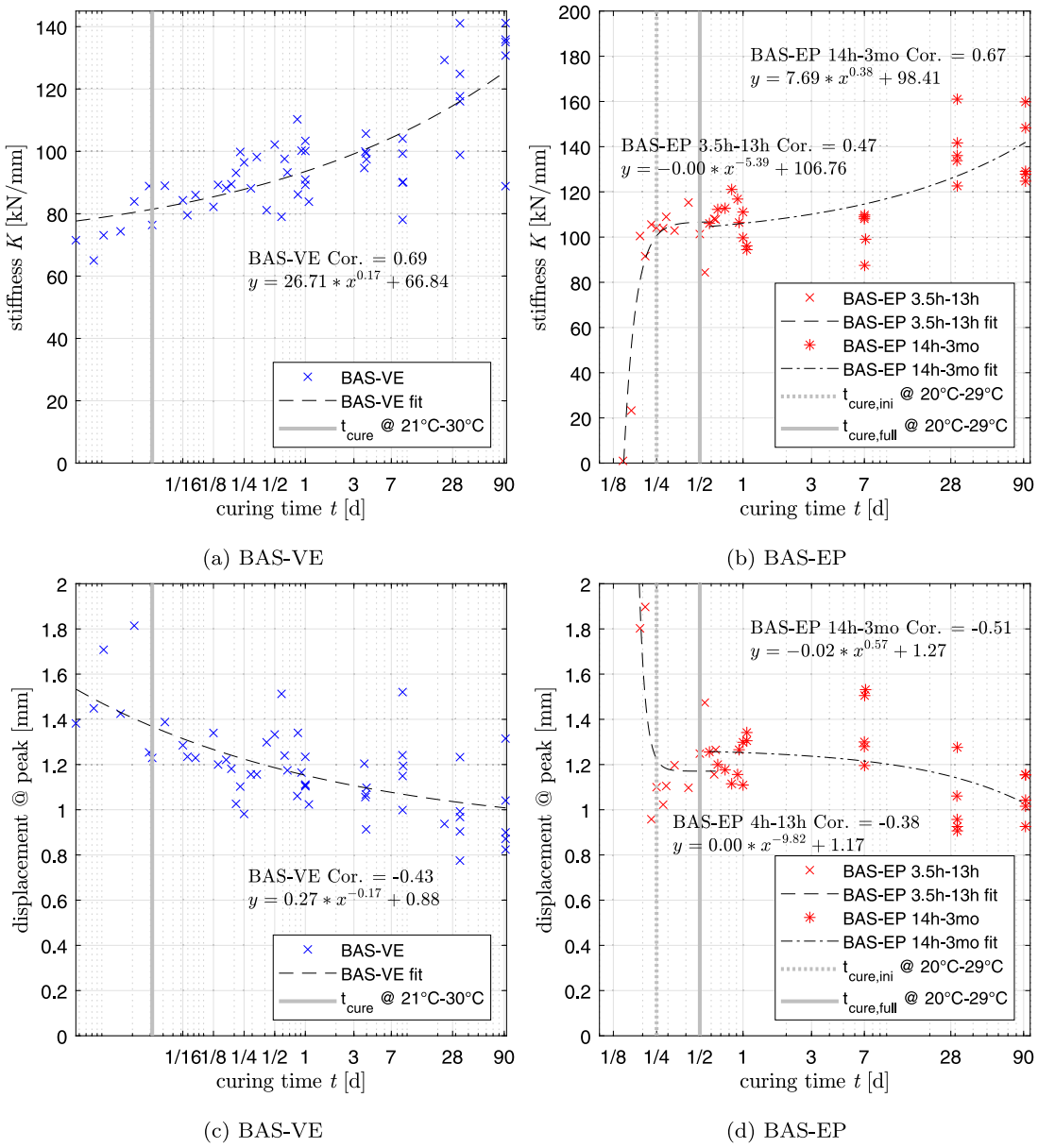

Fig. 5. Evolution of the cure-dependent stiffness and displacement at peak for BAS-VE and BAS-EP. (Vertical gray lines represent the manufacturers' suggested minimum curing times. For BAS-EP the manufacturer defines a "initial" and a "full" curing time). (For interpretation of the references to color in this figure legend, the reader is referred to the web version of this article.)

$$\delta_{CSP} = \frac{\left(\frac{N_{\text{exp}}}{A_{CP}}\right)}{E_{CSP}} h_{CSP} \tag{7}$$

$$\delta_{cor} = \delta_{\text{exp}} - \delta_{TB} - \delta_{CSP} \tag{8}$$

The Young's modulus of the threaded bar, E_{TB}, was experimentally determined in tension tests which confirmed 210 GPa.

5.2. Evolution of the cure-dependent capacity

Cure-dependent capacity is reported by means of the bond strength that is calculated by the uniform bond model (1). In Fig. 4(a) the bond strength of BAS-VE, the vinyl-ester based system, is plotted against the mortar curing time. It is clearly seen that the bond strength values converge promptly. For the very early curing times (tests 8 and 12 min after installation) the bond strength reaches already 78% of the total mean value of all tests (21.97 MPa). Even before reaching the vertical gray line that marks the minimum suggested curing time, the bond strength is already in the range of the tests performed on fully cured systems. The minimum curing time of 45 min is recommended by the manufacturer for a temperature range of the base material between 21–30°C. The bond strength shows a slight increasing, but insignificant trend, after passing a curing time of 15 min. This observation leads to the conclusion, that already 12 to 15 min after the anchor installation, almost the full capacity of the anchor is developed and there is no further significant increase visible.

BAS-EP, the epoxy based system, (Fig. 4(b)) shows a quite different result when the bond strength values are plotted against the curing time. In Fig. 4(b) the bond strength values for curing times (less than 12 h) clearly develop with increasing curing time and can be captured by a power-law function. The dashed vertical gray line marks the manufacturer-specified "initial curing time" (6 h) and the solid vertical gray line represents the "full curing time" (12 h) at a temperature range of 20 °C to 29°C. After the curing time passes, a plateau is visible and the bond strength shows no statistically significant changes in time. We conclude that a safe bond strength value is reached, as described by the manufacturer, at the defined "full curing time" (solid gray line).

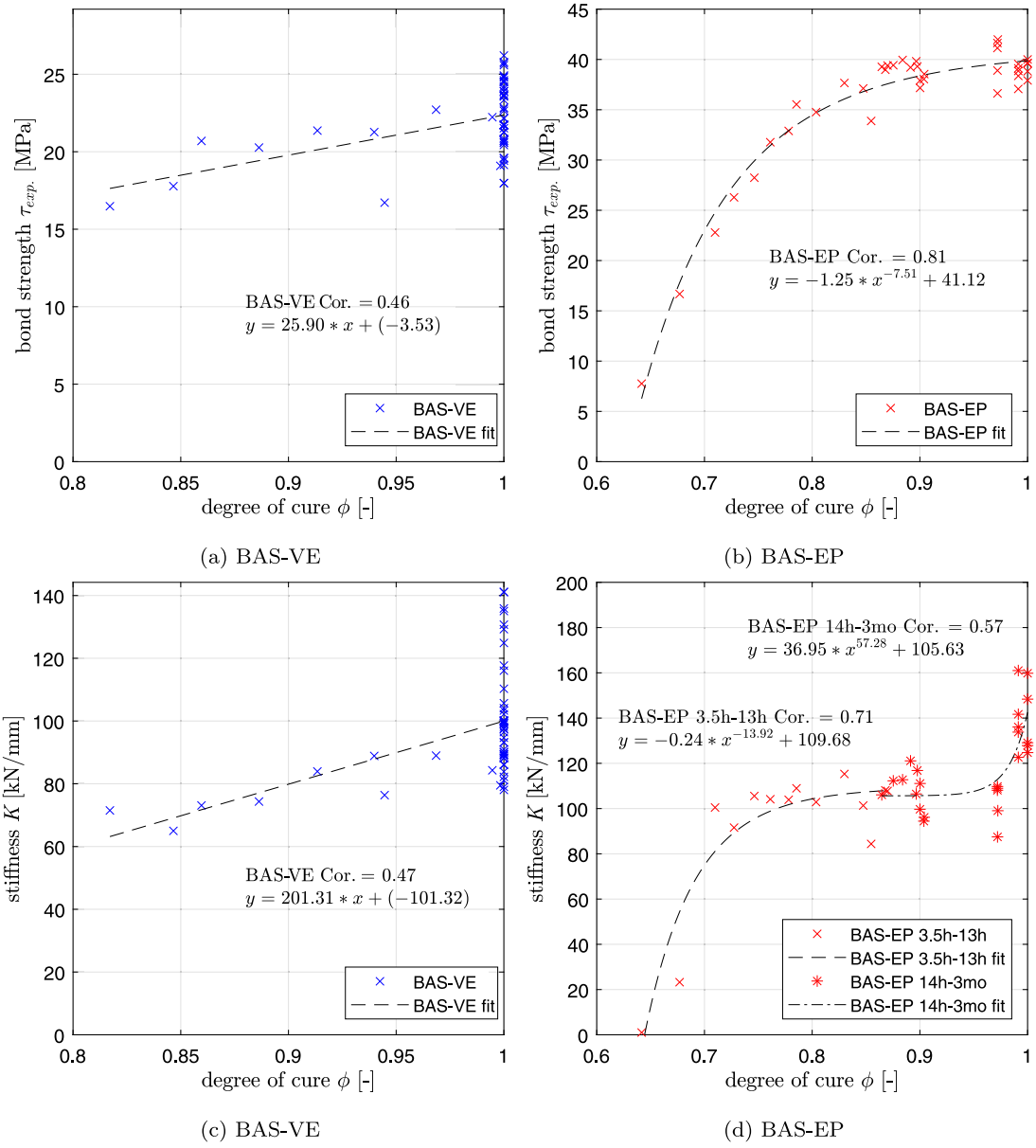

Fig. 6. System response dependency on degree of cure, ϕ.

5.3. Evolution of the cure-dependent stiffness and displacement

For BAS-VE, we present a cure-dependent increase of the system stiffness, K, in Fig. 5(a). This trend is captured by a power-law function. While the difference in stiffness is small for the 1-day and the 7-day tests, a quite substantial increase for the 28-day and 90-day tests is visible. Fig. 5(c) shows a decreasing trend of the displacement at peak (pull-out capacity) with an increasing curing time, following the given power-law function.

In order to capture the system stiffness, K, of BAS-EP, see Fig. 5(b), two power law functions have to be used subsequently. While the stiffness values for very early curing times (before reaching the "initial curing time", dashed gray line) grow substantially, the tests close to the "initial curing time" reach a stable value, which does not show a significant increase up to tests at a curing time of one week. Tests performed 28 and 90 days after installation again show an increased stiffness albeit developing at a different rate, suggesting a different mechanism. Since the adhesive mortar at an age of 1 and 3 months reached, according to the simulation by the curing model, (almost) the fully cured state (ϕ_{1m} = 0.9913 after 1 month, ϕ_{3m} = 1 after 3 months), we assume that the visible increase of the stiffness is not caused by curing. One explanation for the increase in stiffness might lie in long term phenomena related to an uptake (BAS-EP) or loss (BAS-VE) of water as well as solvents in the adhesive mortar, which could be observed in [31,80]. Singer et al. [31] detected weight changes and hydrolytic effects of both adhesives, which lead to changes of the mechanical properties. For vinyl-ester (used in BAS-VE) desorption of water was found, which leads to an increase of the Young's Modulus and might be one part of the explanation of the increasing stiffness. The epoxy-based material (BAS-EP) showed water absorption, which caused a slight reduction in the Young's Modulus.

In Fig. 5(d) the displacement at peak is plotted against the curing time for BAS-EP. It is noticed, that the displacement at peak is first increasing and later decreasing with an increasing curing time. Overall, the measurements at 7 days seem to represent outliers as they are inconsistent with the overall trend and the results obtained on pure material tests.

Table 10
Part 1.

Label	Date DD:MM	Time HH:MM	Temp °C	Humidity %	Date DD:MM	Time HH:MM	Temp °C	Humidity %
	INSTALLATION				TEST			
BAS-VE_8min	05.06.	18:05	23.35	51.50	05.06.	18:13	23.33	51.50
BAS-VE_12min	06.07.	10:37	28.00	51.00	06.07.	10:49	28.03	51.00
BAS-VE_15min	27.05.	08:40	20.33	51.00	27.05.	08:55	20.39	51.00
BAS-VE_22min	06.07.	11:17	28.05	50.00	06.07.	11:39	28.10	47.50
BAS-VE_30min	27.05.	10:24	20.72	50.00	27.05.	10:54	20.87	50.50
BAS-VE_45min	27.05.	08:42	20.34	51.00	27.05.	09:27	20.50	51.00
BAS-VE_45min	05.06.	18:05	23.34	51.50	05.06.	18:47	23.39	51.50
BAS-VE_60min	27.05.	12:24	21.16	47.00	27.05.	13:24	21.36	42.00
BAS-VE_90min	27.05.	08:44	20.35	51.00	27.05.	10:14	20.68	50.00
BAS-VE_100min	06.07.	11:16	28.05	50.00	06.07.	12:56	28.23	46.00
BAS-VE_2h	27.05.	13:26	21.34	42.00	27.05.	15:26	21.51	39.50
BAS-VE_3h	27.05.	08:46	20.35	51.00	27.05.	11:46	21.02	50.50
BAS-VE_200min	06.07.	10:35	27.99	51.00	06.07.	13:55	28.37	41.00
BAS-VE_4h	27.05.	12:26	21.18	51.00	27.05.	16:26	21.94	35.50
BAS-VE_4-5h	06.07.	10:33	27.96	51.00	06.07.	15:03	28.53	41.00
BAS-VE_5h	27.05.	12:30	21.18	47.50	27.05.	17:30	22.30	36.00
BAS-VE_5h	06.06.	10:02	23.68	50.00	06.06.	15:32	24.21	48.50
BAS-VE_6h	27.05.	08:48	20.36	51.00	27.05.	14:48	21.51	40.00
BAS-VE_7h	06.07.	10:31	27.97	51.00	06.07.	17:31	28.55	49.00
BAS-VE_8h	27.05.	10:22	20.70	50.00	27.05.	18:22	22.17	35.50
BAS-VE_10h	27.05.	08:50	20.37	51.00	27.05.	18:50	22.18	35.00
BAS-VE_12h	27.05.	20:00	22.26	37.00	28.05.	08:00	22.60	40.00
BAS-VE_14h	05.06.	18:00	23.32	51.50	06.06.	08:00	23.77	49.00
BAS-VE_15h	27.05.	20:00	22.25	37.00	28.05.	11:00	22.53	42.00
BAS-VE_16h	05.06.	18:02	23.31	51.50	06.06.	10:02	23.68	50.00
BAS-VE_20h	05.06.	18:06	23.35	51.50	06.06.	14:06	24.03	48.50
BAS-VE_20-25h	28.05.	17:00	23.08	44.50	29.05.	13:16	23.35	43.00
BAS-VE_22h	05.06.	18:08	23.33	51.50	06.06.	16:08	24.31	48.00
BAS-VE_1d	27.05.	08:52	20.37	51.00	28.05.	08:52	22.53	41.00
BAS-VE_1d	27.05.	10:20	20.68	50.00	28.05.	10:20	22.44	42.00
BAS-VE_1d	27.05.	12:28	21.18	50.00	28.05.	12:28	22.71	45.00
BAS-VE_1d	27.05.	13:28	21.35	42.00	28.05.	13:28	22.78	47.00
BAS-VE_1d	27.05.	12:34	21.21	47.50	28.05.	14:34	22.89	48.50

5.4. System response dependency on degree of cure

With the aforementioned evolution equation of ϕ, we obtain the degree of cure for both adhesive mortars, BAS-VE and BAS-EP.

We emphasize that the fully cured state ($\phi = 1$) for BAS-VE is reached at a curing time of around 115 min at room temperature. While the curing degree for earlier tests increases almost linearly, it levels off approaching the fully cured state after 115 min. Tests, after this curing state is reached, indeed show no systematic changes in bond strength, see Fig. 4a and Fig. 6a, while the substantial changes in stiffness as observed in Fig. 5a, c result in a comparably large cloud of datapoints at $\phi = 1$, see Fig. 6c.

For BAS-EP, we indeed see a trend in Fig. 6b between the bond strength, τ, plotted against the degree of cure, ϕ. It is seen that the bond strength, τ, follows a power-law function and increases with increasing ϕ as expected. For tests performed at $\phi \geq 0.9$, the bond-strength, τ, levels off. In Fig. 6d, however, the stiffness values, K, demonstrate a substantial increase for the regime of $\phi \geq 0.9$. As for the stiffness-time-relationship in Fig. 5(b), two power law functions are used to capture this phenomenon. Since the curing degree is highly influenced by the curing time, the demonstrated trend is analogous to Fig. 4(b). While the stiffness K for tests with a curing degree ϕ of 0.7 to 0.97 is basically constant, the stiffness for tests with $\phi > 0.99$ is increased, which was already noticed when plotting the stiffness against the curing time, but is even more pronounced for the curing degree in Fig. 6(d), stressing the presence of a second mechanism possibly related to hydrolytic effects, see a recent study on hydrolytic aging effects [81].

6. Conclusions

A large experimental campaign and the corresponding analysis on two commonly used bonded anchor systems were carried out in order to investigate the influence of the mortar-curing effects on the anchor response in a time range from hours to weeks. Therefore, the confined pull-out tests were performed in a range reaching from a few minutes up to three month after anchor installation. For both investigated adhesive mortars a numerical model was developed to numerically retrieve the degree of cure for each structural anchor test. The following conclusions could be drawn:

1. The full anchor capacity by means of pull-out load and bond strength for BAS-VE is reached fast and does not show any significant, cure-dependent increase with time when the minimum curing time according the manufacturer is reached.
2. The anchor capacity increases with time for tests performed at less than 12 h curing time for the epoxy based system (BAS-EP). The approved anchor capacity is reached according the manufacturer given curing times. Longer curing times do not show any significant increase in the anchor capacity.
3. Since both investigated bonded anchor systems reach the approved anchor capacity within the regulated time and temperature regulations, and the current EAD requires compliance with manufacturers' installation instructions, no changes in the assessment practice seem warranted. The further development of anchor properties beyond this point indicates a conservative trend.
4. The anchor stiffness, K, shows an increase with the curing time for BAS-VE, while the displacement at peak is decreasing in a similar manner.
5. While the observed anchor stiffness, K, of BAS-EP close to the approved minimum curing time are quite stable until one week after installation, for later testing ages a strong increase can be observed, especially at 28 and 90 days.
6. For both bonded anchor systems the stiffness is increasing for longer curing times, although the curing process is, according to

Table 11
Part 2.

Label	Date DD:MM	Time HH:MM	Temp °C	Humidity %	Date DD:MM	Time HH:MM	Temp °C	Humidity %
	INSTALLATION				TEST			
BAS-VE_4d	02.07.	17:05	29.32	44.50	06.07.	16:02	28.66	46.50
BAS-VE_4d	02.07.	17:05	29.30	44.50	06.07.	14:25	28.43	41.00
BAS-VE_4d	02.07.	17:05	29.28	44.50	06.07.	15:32	28.64	41.00
BAS-VE_4d	02.07.	17:05	29.29	44.50	06.07.	16:53	28.64	47.00
BAS-VE_4d	02.07.	17:05	29.31	44.50	06.07.	12:12	28.16	46.50
BAS-VE_1w	27.05.	08:54	20.38	51.00	05.06.	09:31	23.50	55.00
BAS-VE_1w	27.05.	10:18	20.67	50.00	05.06.	10:48	23.31	56.00
BAS-VE_1w	27.05.	12:32	21.20	47.50	05.06.	12:32	23.59	54.50
BAS-VE_1w	27.05.	13:30	21.35	40.50	05.06.	14:15	23.74	52.50
BAS-VE_1w	27.05.	12:36	21.22	47.50	05.06.	15:51	23.43	53.00
BAS-VE_3w	06.06.	10:04	23.67	50.00	29.06.	17:17	25.16	68.00
BAS-VE_1mo	27.05.	08:56	20.39	51.00	29.06.	10:53	26.00	68.00
BAS-VE_1mo	27.05.	10:16	20.67	50.00	29.06.	12:05	25.90	72.00
BAS-VE_1mo	27.05.	12:40	21.24	47.50	29.06.	15:34	25.43	73.00
BAS-VE_1mo	27.05.	13:32	21.37	40.50	29.06.	16:06	25.30	73.00
BAS-VE_1mo	27.05.	12:38	21.23	47.50	29.06.	14:31	25.59	72.00
BAS-VE_3mo	30.06.	17:08	27.76	59.00	01.10.	09:45	21.75	53.00
BAS-VE_3mo	30.06.	17:08	27.74	59.00	01.10.	10:51	21.95	50.50
BAS-VE_3mo	30.06.	17:08	27.76	59.00	01.10.	12:44	22.07	50.00
BAS-VE_3mo	30.06.	17:08	27.78	59.00	01.10.	11:52	22.05	50.50
BAS-VE_3mo	30.06.	17:08	27.79	59.00	01.10.	13:06	22.01	50.00
BAS-EP_3-5h	29.05.	08:46	23.60	43.00	29.05.	12:16	23.33	45.50
BAS-EP_4h	29.05.	13:26	23.38	43.00	29.05.	17:26	23.37	47.00
BAS-EP_4-5h	29.05.	13:24	23.35	43.00	29.05.	18:00	23.36	47.00
BAS-EP_5h	29.05.	13:30	23.36	43.50	29.05.	18:30	23.32	51.00
BAS-EP_5-5h	29.05.	08:44	23.60	43.00	29.05.	14:15	23.40	43.50
BAS-EP_6h	29.05.	08:48	23.60	43.00	29.05.	14:48	23.41	45.00
BAS-EP_6-5h	29.05.	09:56	23.36	44.50	29.05.	16:36	23.36	50.50
BAS-EP_7h	29.05.	08:40	23.60	43.00	29.05.	15:40	23.40	50.00
BAS-EP_8h	29.05.	11:22	23.33	46.00	29.05.	19:22	23.26	51.50
BAS-EP_10h	29.05.	09:50	23.39	44.50	29.05.	19:50	23.21	51.00
BAS-EP_12h	29.05.	20:00	23.19	53.50	30.05.	08:00	23.08	40.00

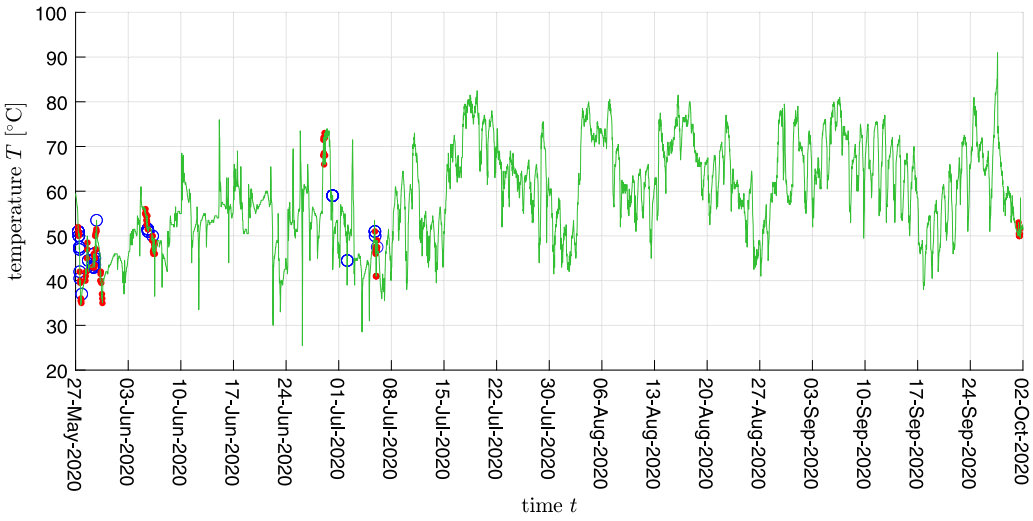

Fig. 7. Recorded ambient humidity history during full campaign. The blue circles mark the installation points and the red dots label the instant of the anchor tests. (For interpretation of the references to color in this figure legend, the reader is referred to the web version of this article.)

the predicted curing degree, (almost) completed. These changes cannot be explained by curing, but may be related to other long term phenomena, which need further investigation.

Although, all anchor pull-out tests carried out according to the manufacturers' specifications reached the regulated values, the investigation could demonstrate cure- and time-dependent influences on the anchor response. As summarized, the pull-out capacity did not significantly change as the approved testing-times were adhered, while the stiffness showed a significant increase with curing time. Since at this time no conclusive explanation for the observed long-term changes could be offered, a further investigations should be considered. Such results could provide much value for future life-cycle and

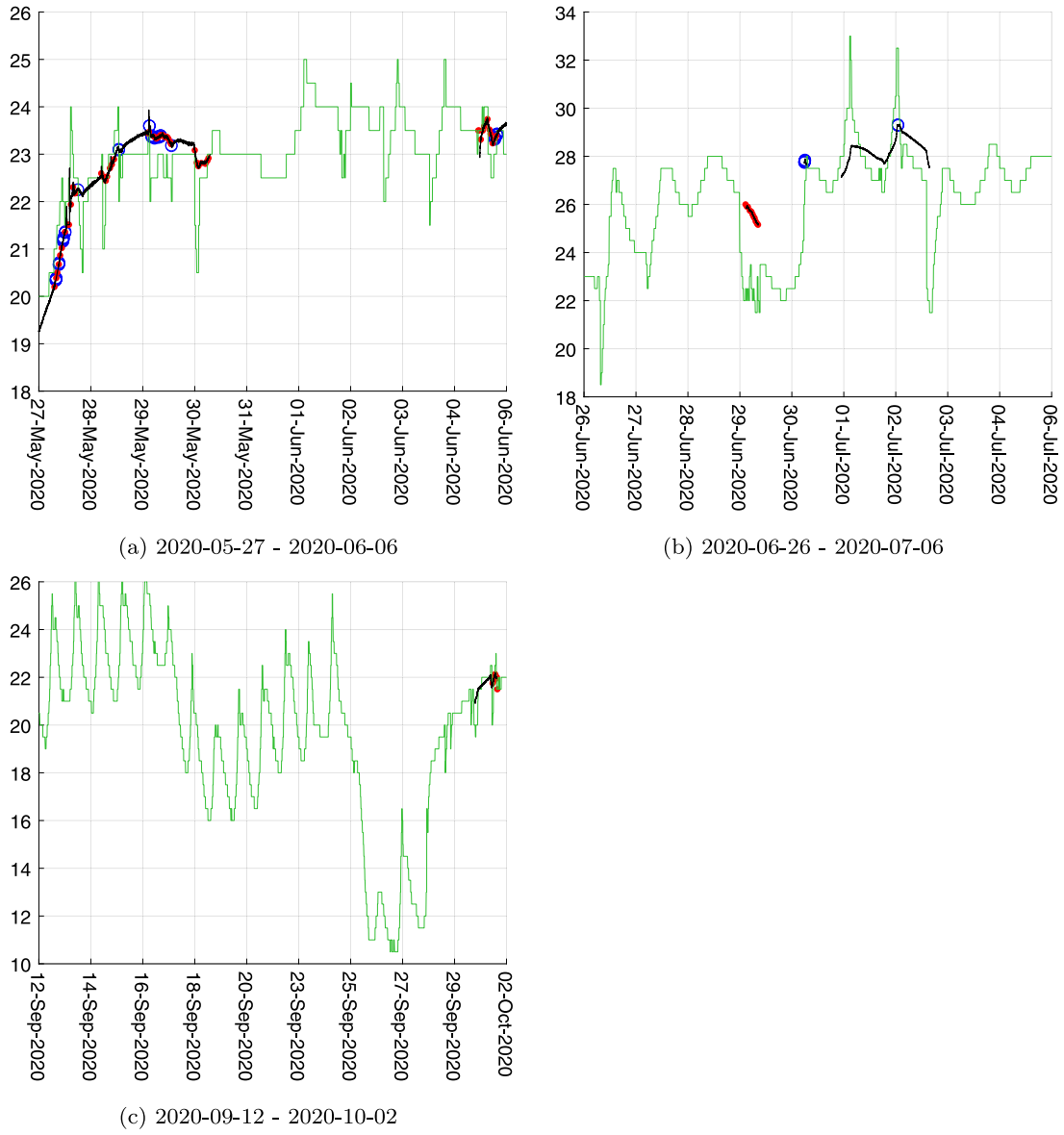

(a) 2020-05-27 - 2020-06-06

(b) 2020-06-26 - 2020-07-06

(c) 2020-09-12 - 2020-10-02

Fig. 8. Enlarged sections of recorded core (black)- and ambient (green) temperature history during full campaign. Full history provided in Fig. 3.

robustness assessments of bonded anchors, especially if based on numerical modeling.

CRediT authorship contribution statement

Stefan Meißl: Conceptualization, Methodology, Experiments, Writing – original draft. **Krešimir Ninčević:** Conceptualization, Methodology, Writing - review. **Bilen Emek Abali:** Modeling, Writing – review & editing. **Roman Wan-Wendner:** Conceptualization, Methodology, Writing – review & editing, Supervision.

Declaration of competing interest

The authors declare that they have no known competing financial interests or personal relationships that could have appeared to influence the work reported in this paper.

Data availability

Data will be made available on request.

Acknowledgments

This research was funded by the Christian Doppler Forschungsgesellschaft, Austria, Grant LICROFAST to Roman Wan-Wendner. The financial support by the Austrian Federal Ministry for Digital and Economic Affairs and the National Foundation for Research, Technology, and Development is acknowledged, as is the partial financial support by the Austrian Science Fund (FWF) under Grant P 31203-N32.

Lorenz Nagl is gratefully acknowledged for his support during performing the anchor pull-out tests. The support by Lisa Sinn, Gilda Daissè, Michele Zechini and Ioannis Boumakis as well as the laboratory team and the involved students during specimen preparation is thankfully acknowledged, so is their contribution for the material characterization.

Table 12
Part 3.

Label	Date DD:MM	Time HH:MM	Temp °C	Humidity %	Date DD:MM	Time HH:MM	Temp °C	Humidity %
	INSTALLATION				TEST			
BAS-EP_13h	29.05.	20:02	23.17	53.50	30.05.	09:02	22.82	41.50
BAS-EP_14h	05.06.	19:00	23.41	51.00	06.06.	09:00	23.68	49.00
BAS-EP_15h	28.05.	17:00	23.10	44.50	29.05.	08:06	23.44	43.00
BAS-EP_15h	28.05.	17:00	23.11	44.50	29.05.	08:29	23.47	43.00
BAS-EP_16h	05.06.	19:02	23.41	51.00	06.06.	11:02	23.71	46.50
BAS-EP_18h	05.06.	19:04	23.43	51.00	06.06.	13:04	23.90	47.00
BAS-EP_20h	05.06.	19:06	23.43	51.00	06.06.	15:06	24.16	48.00
BAS-EP_22h	05.06.	19:08	23.40	51.00	06.06.	17:08	24.58	46.00
BAS-EP_1d	29.05.	09:52	23.38	44.50	30.05.	11:22	22.81	39.50
BAS-EP_1d	29.05.	11:20	23.35	46.00	30.05.	09:52	22.75	42.00
BAS-EP_1d	29.05.	13:28	23.37	43.00	30.05.	13:28	22.80	37.00
BAS-EP_1d	29.05.	14:28	23.37	43.50	30.05.	14:28	22.86	36.00
BAS-EP_1d	29.05.	13:34	23.36	43.50	30.05.	15:04	22.92	35.00
BAS-EP_1w	29.05.	09:54	23.37	44.50	05.06.	09:54	23.50	55.00
BAS-EP_1w	29.05.	11:18	23.35	46.00	05.06.	11:48	23.50	55.00
BAS-EP_1w	29.05.	13:32	23.36	43.50	05.06.	13:32	23.67	53.50
BAS-EP_1w	29.05.	14:30	23.40	45.00	05.06.	15:15	23.52	53.50
BAS-EP_1w	29.05.	13:36	23.37	43.50	05.06.	16:51	23.23	54.50
BAS-EP_1mo	29.05.	14:26	23.38	43.50	29.06.	11:34	25.91	71.50
BAS-EP_1mo	29.05.	11:16	23.35	46.00	29.06.	13:04	25.75	68.50
BAS-EP_1mo	29.05.	13:40	23.36	43.50	29.06.	13:54	25.70	66.00
BAS-EP_1mo	29.05.	14:32	23.39	45.00	29.06.	16:48	25.21	72.00
BAS-EP_1mo	29.05.	13:38	23.36	43.50	29.06.	15:02	25.49	72.00
BAS-EP_3mo	30.06.	17:19	27.84	59.00	01.10.	11:27	22.01	50.00
BAS-EP_3mo	30.06.	17:19	27.83	59.00	01.10.	13:31	21.95	50.00
BAS-EP_3mo	30.06.	17:19	27.82	59.00	01.10.	14:05	22.00	50.50
BAS-EP_3mo	30.06.	17:19	27.82	59.00	01.10.	14:35	21.50	51.50
BAS-EP_3mo	30.06.	17:19	27.85	59.00	01.10.	12:20	22.13	50.00
BAS-EP_3mo	30.06.	17:19	27.85	59.00	01.10.	10:20	21.82	52.00

Annex

See Tables 10–12 and Figs. 7 and 8.

References

[1] R. Eligehausen, R. Mallée, F.S. Silva, Anchorage in Concrete Construction, first ed., Ernst & Sohn, 2006.

[2] R.A. Cook, J. Kunz, W. Fuchs, R.C. Konz, Behavior and design of adhesive bonded anchors, ACI Struct. J. 103 (6) (2006) 822–831.

[3] R.A. Sauer, A survey of computational models for adhesion, J. Adhes. 92 (2) (2016) 81–120.

[4] I. Boumakis, M. Marcon, K. Nincevic, L.-M. Czernuschka, R. Wan-Wendner, Concrete creep effect on bond stress in adhesive fastening systems, in: 3rd International Symposium on Connections Between Steel and Concrete, 2017, pp. 396–406.

[5] J. Podroužek, J. Vorel, R. Wan-Wendner, Design for lifecycle robustness of fastening systems, Beton-Und Stahlbetonbau 113 (2018) 62–66.

[6] R. Wan-Wendner, J. Podroužek, Robust power law extrapolation for adhesive anchors under sustained load., ACI Struct. J. 116 (1) (2019).

[7] R. Wendner, K. Nincevic, I. Boumakis, L. Wan, Age-dependent lattice discrete particle model for quasi-static simulations, Key Eng. Mater. 711 (2016) 1090–1097, http://dx.doi.org/10.4028/www.scientific.net/KEM.711.1090, URL https://www.scientific.net/KEM.711.1090.

[8] L. Wan-Wendner, R. Wan-Wendner, G. Cusatis, Age-dependent size effect and fracture characteristics of ultra high performance concrete, Cem. Concr. Compos. 85 (2016) http://dx.doi.org/10.1016/j.cemconcomp.2017.09.010.

[9] H. Hong, Assessment of reliability of aging reinforced concrete structures, J. Struct. Eng. 126 (12) (2000) 1458–1465.

[10] C. Wang, Q. Li, B.R. Ellingwood, Time-dependent reliability of ageing structures: an approximate approach, Struct. Infrastruct. Eng. 12 (12) (2016) 1566–1572.

[11] L. Wan, R. Wendner, B. Liang, G. Cusatis, Analysis of the behavior of ultra high performance concrete at early age, Cem. Concr. Compos. 74 (2016) 120–135.

[12] L. Czernuschka, K. Ninčević, I. Boumakis, L. Wan-Wendner, R. Wan-Wendner, Aging Behavior of Normal and High Strength Concretes, 2018, pp. 197–202, http://dx.doi.org/10.1201/9781315182964-24.

[13] A. González, A. Barrias, R. Teixeira, D. Martinez, B. Heitner, S. Antonopoulou, G. Zou, A. Gonzalez Merino, S.N.A. Sourav, J.R. Casas, et al., TRUSS, a European innovative training network dealing with the challenges of an aging infrastructure network, in: The 7th Asia-Pacific Workshop on Structural Health Monitoring (APWSHM 2018), Hong Kong, China, 12-15 November 2018, 2018.

[14] S.-G. Kim, Y.-S. Park, Y.-H. Lee, Rate-type age-dependent constitutive formulation of concrete loaded at an early age, Materials 12 (3) (2019) 514.

[15] F.-J. Ulm, G. Constantinides, F. Heukamp, Is concrete a poromechanics materials?—A multiscale investigation of poroelastic properties, Mater. Struct. 37 (1) (2004) 43–58.

[16] E. Aigner, R. Lackner, C. Pichler, Multiscale prediction of viscoelastic properties of asphalt concrete, J. Mater. Civ. Eng. 21 (12) (2009) 771–780.

[17] J.F. Unger, S. Eckardt, Multiscale modeling of concrete, Arch. Comput. Methods Eng. 18 (3) (2011) 341.

[18] L. Contrafatto, M. Cuomo, S. Gazzo, A concrete homogenisation technique at meso-scale level accounting for damaging behaviour of cement paste and aggregates, Comput. Struct. 173 (2016) 1–18.

[19] I. Giorgio, D. Scerrato, Multi-scale concrete model with rate-dependent internal friction, Eur. J. Environ. Civ. Eng. 21 (7–8) (2017) 821–839.

[20] D. Scerrato, I. Giorgio, A. Della Corte, A. Madeo, N. Dowling, F. Darve, Towards the design of an enriched concrete with enhanced dissipation performances, Cem. Concr. Res. 84 (2016) 48–61.

[21] D. Scerrato, I. Giorgio, A. Della Corte, A. Madeo, A. Limam, A micro-structural model for dissipation phenomena in the concrete, Int. J. Numer. Anal. Methods Geomech. 39 (18) (2015) 2037–2052.

[22] S.Y. Alam, A. Loukili, Transition from energy dissipation to crack openings during continuum–discontinuum fracture of concrete, Int. J. Fract. 206 (1) (2017) 49–66.

[23] B. Chiaia, O. Kumpyak, L. Placidi, V. Maksimov, Experimental analysis and modeling of two-way reinforced concrete slabs over different kinds of yielding supports under short-term dynamic loading, Eng. Struct. 96 (2015) 88–99.

[24] F. dell'Isola, A.M. Bragov, L.A. Igumnov, B.E. Abali, A.K. Lomunov, D.A. Lamzin, A.Y. Konstantinov, Mechanical response change in fine grain concrete under high strain and stress rates, in: New Achievements in Continuum Mechanics and Thermodynamics, Springer, 2019, pp. 71–80.

[25] J.G. Van Mier, Concrete Fracture: A Multiscale Approach, CRC Press, 2012.

[26] K. Ninčević, L.-M. Czernuschka, I.B. Marco Marcon, R. Wan-Wendner, Aggregate effect in fastening applications, in: 39th IABSE Symposium - Engineering the Future - September 21-23 2017, Vancouver, Canada, 2017.

[27] M. Marcon, K. Ninčević, I. Boumakis, L. Czernuschka, R. Wan-Wendner, Aggregate effect on the concrete cone capacity of an undercut anchor under quasi-static tensile load, Materials 11 (2018) 711, http://dx.doi.org/10.3390/ma11050711.

[28] K. Ninčević, L.-M. Czernuschka, M. Marcon, R. Wan-Wendner, Age and cure dependence of concrete cone capacity in tension, ACI Struct. J. 116 (4) (2019) http://dx.doi.org/10.14359/51715575.

[29] K. Ninčević, I. Boumakis, M. Marcon, R. Wan-Wendner, Aggregate effect on concrete cone capacity, Eng. Struct. 191 (2019) 358–369, http://dx.doi.org/10.1016/j.engstruct.2019.04.028, URL http://www.sciencedirect.com/science/article/pii/S0141029618327470.

[30] K. Ninčević, R. Wan-Wendner, On the dependence of concrete edge breakout on concrete age and coarse aggregate type, Struct. Concr. 22 (5) (2021) 2952–2966, http://dx.doi.org/10.1002/suco.202000653, arXiv:https://onlinelibrary.wiley.com/doi/pdf/10.1002/suco.202000653, URL https://onlinelibrary.wiley.com/doi/abs/10.1002/suco.202000653.

[31] G. Singer, G. Sinn, K. Schwendtner, H.C. Lichtenegger, R. Wan-Wendner, Time-dependent changes of mechanical properties of polymer-based composite materials for adhesive anchor systems, Compos. Struct. 196 (2018) 155–162, http://dx.doi.org/10.1016/j.compstruct.2018.04.076, URL <Go to ISI>://WOS:000433205200015.

[32] G. Daissè, M. Marcon, M. Zecchini, R. Wan-Wendner, Cure-dependent loading rate effects on strength and stiffness of particle-reinforced thermoset polymers, Polymer 259 (2022) 125326, http://dx.doi.org/10.1016/j.polymer.2022.125326, URL https://www.sciencedirect.com/science/article/pii/S0032386122008138.

[33] Z. Liao, M. Hossain, X. Yao, M. Mehnert, P. Steinmann, On thermo-viscoelastic experimental characterisation and numerical modelling of VHB polymer, Int. J. Non-Linear Mech. (2019) 103263.

[34] G. Singer, G. Sinn, H.C. Lichtenegger, S. Veigel, M. Zecchini, R. Wan-Wendner, Evaluation of in-situ shrinkage and expansion properties of polymer composite materials for adhesive anchor systems by a novel approach based on digital image correlation, Polym. Test. 79 (2019) 8, http://dx.doi.org/10.1016/j.polymertesting.2019.106035, URL <Go to ISI>://WOS:000499945200027.

[35] P.R. Bradler, J. Fischer, R. Wan-Wendner, R.W. Lang, Shear test equipment for testing various polymeric materials by using standardized multipurpose specimens with minor adaptions, Polym. Test. 75 (2019) 93–98.

[36] J. Fischer, P.R. Bradler, D. Schmidtbauer, R.W. Lang, R. Wan-Wendner, Long-term creep behavior of resin-based polymers in the construction industry, Mater. Today Commun. 18 (2019) 60–65, http://dx.doi.org/10.1016/j.mtcomm.2018.11.006, URL <Go to ISI>://WOS:000456868200009.

[37] I. Boumakis, M. Marcon, K. Nincevic, L.M. Czernuschka, R. Wan-Wendner, Concrete creep and shrinkage effect in adhesive anchors subjected to sustained loads, Eng. Struct. 175 (2018) 790–805, URL <Go to ISI>://WOS:000448101300053.

[38] I. Boumakis, K. Nincevic, J. Vorel, R. Wan-Wendner, Creep rate based time-to-failure prediction of adhesive anchor systems under sustained load, Composites B 178 (2019) 14, http://dx.doi.org/10.1016/j.compositesb.2019.107389, URL <Go to ISI>://WOS:000498274700001.

[39] K. Ninčević, I. Boumakis, S. Meissl, R. Wan-Wendner, Consistent time-to-failure tests and analyses of adhesive anchor systems, Appl. Sci. 10 (4) (2020) 1527, URL https://www.mdpi.com/2076-3417/10/4/1527.

[40] EOTA, European assessement document - bonded fasteners for use in concrete, 2018, p. 115, URL https://www.eota.eu.

[41] EOTA, Details of tests for post-installed fasteners in concrete; European organization for technical approvals, TR048, 2016, p. 27, URL https://www.eota.eu.

[42] R.A. Cook, Behavior of chemically bonded anchors, J. Struct. Eng. 119 (9) (1993) 2744–2762, http://dx.doi.org/10.1061/(ASCE)0733-9445(1993)119:9(2744).

[43] R.A. Cook, J. Kunz, W. Fuchs, R.C. Konz, Behavior and design of single adhesive anchors under tensile load in uncracked concrete, ACI Struct. J. 95 (1) (1998) 9–26.

[44] R.A. Cook, E.P. Douglas, T.M. Davis, C. Liu, NCHRP report 757: Long-term performance of epoxy adhesive anchor systems, Report, 2013.

[45] CEN, BS EN 1992-1-1:2004 Eurocode 2: Design of Concrete Structures - Part 1-1: General Rules and Rules for Buildings, European Committee for Standardization.

[46] fib, Fib Model Code for Concrete Structures 2010, International Federation for Structural Concrete.

[47] B. Yagimli, A. Lion, Experimental investigations and material modelling of curing processes under small deformations, ZAMM Z. Angew. Math. Mech. 91 (5) (2011) 342–359.

[48] B.E. Abali, J. Vorel, R. Wan-Wendner, Thermo-mechano-chemical modeling and computation of thermosetting polymers used in post-installed fastening systems in concrete structures, Contin. Mech. Thermodyn. (2020) 1–20.

[49] M. Hossain, P. Steinmann, Modelling and simulation of the curing process of polymers by a modified formulation of the Arruda–Boyce model, Arch. Mech. 63 (5–6) (2011) 621–633.

[50] M. André, P. Wriggers, Thermo-mechanical behaviour of rubber materials during vulcanization, Int. J. Solids Struct. 42 (16–17) (2005) 4758–4778.

[51] R. Mahnken, Thermodynamic consistent modeling of polymer curing coupled to visco–elasticity at large strains, Int. J. Solids Struct. 50 (13) (2013) 2003–2021.

[52] H. Dal, C. Zopf, M. Kaliske, Micro-sphere based viscoplastic constitutive model for uncured green rubber, Int. J. Solids Struct. 132 (2018) 201–217.

[53] M. Johlitz, A. Lion, Chemo-thermomechanical ageing of elastomers based on multiphase continuum mechanics, Contin. Mech. Thermodyn. 25 (5) (2013) 605–624.

[54] T.-T. Nguyen, D. Waldmann, T.Q. Bui, Phase field simulation of early-age fracture in cement-based materials, Int. J. Solids Struct. (2019).

[55] S. Klinge, A. Bartels, P. Steinmann, The multiscale approach to the curing of polymers incorporating viscous and shrinkage effects, Int. J. Solids Struct. 49 (26) (2012) 3883–3900.

[56] S. Klinge, K. Hackl, Application of the multiscale FEM to the modeling of nonlinear composites with a random microstructure, Int. J. Multiscale Comput. Eng. 10 (3) (2012).

[57] F. Otero, S. Oller, X. Martinez, Multiscale computational homogenization: review and proposal of a new enhanced-first-order method, Arch. Comput. Methods Eng. 25 (2) (2018) 479–505.

[58] T. Zohdi, P. Wriggers, Phenomenological modeling and numerical simulation of the environmental degradation of multiphase engineering materials, Arch. Appl. Mech. 70 (1–3) (2000) 47–64.

[59] M. Hossain, G. Possart, P. Steinmann, A small-strain model to simulate the curing of thermosets, Comput. Mech. 43 (6) (2009) 769–779.

[60] M. Hossain, P. Steinmann, Degree of cure-dependent modelling for polymer curing processes at small-strain. Part I: consistent reformulation, Comput. Mech. 53 (4) (2014) 777–787.

[61] M. Hossain, G. Possart, P. Steinmann, A finite strain framework for the simulation of polymer curing. Part I: elasticity, Comput. Mech. 44 (5) (2009) 621–630.

[62] M. Hossain, G. Possart, P. Steinmann, A finite strain framework for the simulation of polymer curing. Part II. Viscoelasticity and shrinkage, Comput. Mech. 46 (3) (2010) 363–375.

[63] T. Sain, K. Loeffel, S. Chester, A thermo–chemo–mechanically coupled constitutive model for curing of glassy polymers, J. Mech. Phys. Solids 116 (2018) 267–289.

[64] R. Landgraf, M. Rudolph, R. Scherzer, J. Ihlemann, Modelling and simulation of adhesive curing processes in bonded piezo metal composites, Comput. Mech. 54 (2) (2014) 547–565.

[65] S. Hu, Y. Chen, A FEM coupling model for properties prediction during the curing of an epoxy adhesive for a novel assembly of radio telescope panel, in: Advances in Optical and Mechanical Technologies for Telescopes and Instrumentation, Vol. 9151, International Society for Optics and Photonics, 2014, 915132.

[66] C. Leistner, S. Hartmann, D. Abliz, G. Ziegmann, Modeling and simulation of the curing process of epoxy resins using finite elements, Contin. Mech. Thermodyn. 32 (2) (2020) 327–350.

[67] M. Kiasat, Curing shrinkage and residual stresses in viscoelastic thermosetting resins and composites, (Ph.D. thesis), Technical University of Delft, 2000.

[68] R. Landgraf, Modellierung und simulation der aushärtung polymerer werkstoffe, (Ph.D. thesis), Technical University of Chemnitz, 2016.

[69] L. Shechter, J. Wynstra, R.P. Kurkjy, Glycidyl ether reactions with amines, Ind. Eng. Chem. 48 (1) (1956) 94–97.

[70] M.R. Kamal, Thermoset characterization for moldability analysis, Polym. Eng. Sci. 14 (3) (1974) 231–239.

[71] C. Heinrich, M. Aldridge, A.S. Wineman, J. Kieffer, A.M. Waas, K.W. Shahwan, Generation of heat and stress during the cure of polymers used in fiber composites, Internat. J. Engrg. Sci. (53) (2012) 85–111.

[72] B.E. Abali, M. Zecchini, G. Daissè, I. Czabany, W. Gindl-Altmutter, R. Wan-Wendner, Cure kinetics and inverse analysis of epoxy-amine based adhesive used for fastening systems, Materials 14 (14) (2021) 3853, http://dx.doi.org/10.3390/ma14143853, URL https://www.mdpi.com/1996-1944/14/14/3853.

[73] B.E. Abali, M.Y. Yardımcı, M. Zecchini, G. Daissè, F.H. Marchesini, G. De Schutter, R. Wan-Wendner, Experimental investigation for modeling the hardening of thermosetting polymers during curing, Polym. Test. 102 (2021) 107310, http://dx.doi.org/10.1016/j.polymertesting.2021.107310, URL https://www.sciencedirect.com/science/article/pii/S0142941821002579.

[74] H.-J. Flammersheim, J.R. Opfermann, Investigation of epoxide curing reactions by differential scanning calorimetry–formal kinetic evaluation, Macromol. Mater. Eng. 286 (3) (2001) 143–150.

[75] C.-S. Chern, G.W. Poehlein, A kinetic model for curing reactions of epoxides with amines, Polym. Eng. Sci. 27 (11) (1987) 788–795.

[76] D. Hesekamp, H.C. Broecker, M.H. Pahl, Chemo-rheology of cross-linking polymers, Chem. Eng. Technol.: Ind. Chem.-Plant Equipment-Process Eng.-Biotechnol. 21 (2) (1998) 149–153.

[77] C.W. Wise, W.D. Cook, A.A. Goodwin, Chemico-diffusion kinetics of model epoxy-amine resins, Polymer 38 (13) (1997) 3251–3261.

[78] R. Venditti, J. Gillham, A relationship between the glass transition temperature (Tg) and fractional conversion for thermosetting systems, J. Appl. Polym. Sci. 64 (1) (1997) 3–14.

[79] E. Rabinowitch, Collision, co-ordination, diffusion and reaction velocity in condensed systems, Trans. Faraday Soc. 33 (1937) 1225–1233.

[80] P. Siedlaczek, G. Sinn, P. Peter, R. Wan-Wendner, H.C. Lichtenegger, Characterization of moisture uptake and diffusion mechanisms in particle-filled composites, Polymer 249 (2022) 124799, http://dx.doi.org/10.1016/j.polymer.2022.124799, URL https://www.sciencedirect.com/science/article/pii/S0032386122002865.

[81] P. Siedlaczek, G. Sinn, P. Peter, J. Jandl, G. Hantal, K. Wriessnig, R. Wan-Wendner, H.C. Lichtenegger, Hygrothermal aging of particle-filled epoxy-based composites, 2022, Preprint Submitted.